Article

The International Journal of
Robotics Research
2015, Vol. 34(11) 1347–1360

DOI: 10.1177/0278364914558494
ijr.sagepub.com
SAGE

Stable, open-loop precision manipulation with underactuated hands

Lael U. Odhner and Aaron M. Dollar

Abstract

This paper discusses dexterous, within-hand manipulation with differential-type underactuated hands. We discuss the fact that not only can this class of hands, which to date have been considered almost exclusively for adaptive grasping, be utilized for precision manipulation, but also that the reduction of the number of actuators and constraints can make within-hand manipulation easier to implement and control. Next, we introduce an analytical framework for evaluating the dexterous workspace of objects held within the fingertips in a precision grasp. A set of design principles for underactuated fingers are developed that enable fingertip grasping and manipulation. Finally, we apply this framework to analyze the workspace of stable object configurations for an object held within a pinch grasp of a two-fingered underactuated planar hand, demonstrating a large and useful workspace despite only one actuator per finger. The in-hand manipulation workspace for the iRobot–Harvard–Yale Hand is experimentally measured and presented.

Keywords

Dexterous manipulation, manipulation, mechanism design, mechanics, design and control, underactuated robots

1. Introduction

Manipulating an object held between the fingers of a robotic hand is extraordinarily difficult: each finger must move so that a sufficient number of fingertips maintain continuous contact with the object, while exerting forces that ensure a stable grasp (Michelman, 1998). These conditions can be expensive to measure and control directly, and the hardware complexity required for direct sensing and control often introduce new sources of error. One strategy for limiting the amount of data required to successfully complete tasks of this kind is to simplify the problem using passive mechanisms. A good hardware design can often reduce the task's success criteria to a simpler set of success criteria, reducing the amount of knowledge that must be collected.

Robotic grasping, a problem closely related to in-hand manipulation, provides many examples of how a complex set of necessary conditions can be simplified through the correct choice of mechanism. Obtaining a successful grasp on a rigid object is often posed as a free body diagram; each contact between a gripper and an object exerts some wrench on the object, and an object is considered to be stably grasped when the sum of these wrenches can be controlled to resist any anticipated external disturbance (Mason and Salisbury, 1985). These contact forces need not be measured or controlled directly in order to keep the object in equilibrium, though. Many underactuated grippers have been shown to successfully grasp objects despite having limited sensing and control authority (Ulrich et al., 1988; Crisman et al., 1996; Birglen et al., 2008; Dollar and Howe, 2009; Robotiq, 2013; Kinova Robotics, 2013; Aukes et al., 2014). Underactuated hands resist external disturbance forces by exploiting internal constraints on the hand and object. The fingers passively wrap around an object to obtain an encircling grasp. Once the finger links have fully made contact with the object, the hand–object contacts act as parallel constraints, so that hand and object are rigidly assembled into a fully constrained or overconstrained virtual linkage. By tuning the kinematic properties of the underactuated transmission, only a small number of actuators are required to exert the inward forces holding the hand and object together (Hirose and Umetani, 1978).

In this paper, we will demonstrate that the mechanisms used in underactuated, passively adaptive grippers can also be tuned to make in-hand manipulation possible with

Department of Mechanical Engineering and Materials Sciences, Yale University, USA

Corresponding author:
Aaron Dollar, Yale University, 15 Prospect St., New Haven, CT 06511, USA.
Email: aaron.dollar@yale.edu

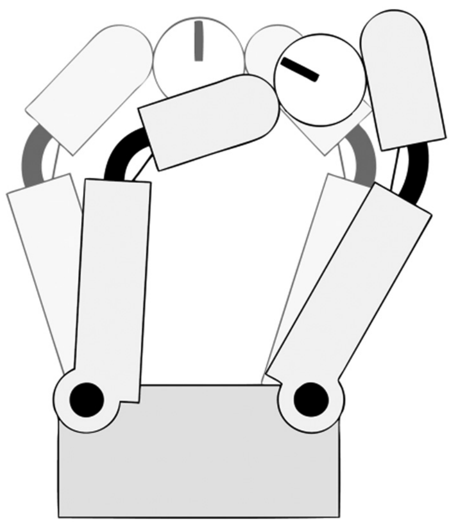

Fig. 1. An underactuated hand can be used to grasp and manipulate objects without the need for complex sensing.

minimal sensing. Figure 1 illustrates the process of “precision manipulation” (Okamura et al., 2000, Ma and Dollar, 2011): an object is pinched between two fingertips, and held in equilibrium while the fingers are moved in a combination of rolling and pinching motions. Utilizing the specially-designed mechanics of our underactuated hands, no force sensing is required for the task, due to the novel tuning of the fingertip mechanics. We will examine theoretical parallels between grasping and fingertip manipulation using underactuated hands, and show that underactuated hands can be developed with underactuated manipulation in mind. Performance limitations due to underactuation will be discussed, such as reduction in range of motion. Additional design criteria will be presented, along with success metrics, such as the compliance and contact force sensitivity matrices. Finally, experimental results will be shown, demonstrating that underactuated in-hand manipulation is achievable in practice.

1.1. Background

Underactuated hands are designed to have fewer actuators than articulated joints. The motions of the joints are coupled through tendon or linkage transmissions, and are usually assembled with elastic elements that cause the hand to move repeatably by keeping the hand in a quasi-static equilibrium configuration. The majority of extant underactuated hands have been built for simple grasping tasks, such as power grasping objects of unknown size (e.g. Birglen et al., 2008; Dollar and Howe, 2009), or obtaining a pinch grasp on a small object (e.g. Kragten and Herder, 2010; Aukes et al., 2014). However, dexterous precision manipulation with differential-type underactuated hands has yet to be examined in depth.

Several researchers have considered fingertip manipulation with hands incorporating series elastic actuators (SEAs) without differential transmission of actuation, which are sometimes also referred to as underactuated. For example, several hands using SEAs or variable impedance actuators have been built (e.g. Edsinger-Gonzales and Weber, 2004; Grebenstein et al., 2012). Prattichizzo et al. (2012a) have shown that the passive behavior of the series elastic elements can be used to independently control force and motion in this kind of hand. Elastic elements placed in series with actuation synergies (motions coupled across multiple joints in a hand) have been proposed, and the local manipulability of these hands has been analyzed (Prattichizzo et al., 2012b). The instantaneous mobility of closed-chain underactuated structures has also been analyzed (Quennouelle and Gosselin, 2009), although the analysis requires a closed-form expression for parallel kinematic constraints, and so is not completely applicable to the problem of fingertip grasping. The work described in this paper extends preliminary work by the authors on the topic (Odhner and Dollar, 2011; Odhner et al., 2013). This more complete paper provides more background on the connection between underactuated grasping and manipulation, and contains more comprehensive results based on a new hardware platform, the iRobot–Harvard–Yale (iHY) Hand developed by the authors in collaboration for the DARPA ARM-H program (Odhner et al., 2014).

This paper is organized into several sections. We begin in Section 2 by overviewing the iHY Hand, and introducing a model and terminology for later discussion. Section 3 examines the theoretical and practical considerations that go into designing an underactuated hand for pinch grasping and fingertip manipulation. Sufficient conditions for elastic stability and manipulability are derived, and the analysis shows that the frictional contact constraints and actuation constraints on the hand play a crucial role in determining these, along with the elastic energy associated with the motion of the robot hand. The dominant physical phenomena behind these determining factors are considered to create rules for mechanism design, avoiding reliance on fine-grained models for design optimization. Section 4 then demonstrates how an a priori prediction of the reachable space of manipulated object configurations can be computed for a pinched object using the hand–object model. The prediction is compared to measured results from the iHY Hand.

2. Apparatus, modeling and terminology

2.1 The iRobot–Harvard–Yale Hand

The iHY Hand is a low-cost, intermediate-dexterity robot hand developed by the authors in collaboration with iRobot Corporation and the Harvard BioRobotics Laboratory (Odhner et al., 2014). This hand, depicted in Figure 2, is a three-fingered gripper capable of reconfiguring between an interdigitated grasp (shown) and a two-finger opposed pinch grasp. The fingers of the iHY Hand are independent and differentially underactuated, having only a single flexor

Fig. 2. The iRobot–Harvard–Yale Hand, an underactuated hand designed for both power grasps and pinch grasps, and in-hand manipulation.

tendon per finger inserted across both the proximal and distal joints. This hand is similar in many respects to previous underactuated hands, but novel in its ability to grasp with the tips of the fingers without relying on hard stops, clutches, brakes or similar locking mechanisms. In this paper, we will see that the ability to grasp without locking the fingers is a key to achieving robust in-hand manipulation.

Figure 3 shows the fingers of the iHY Hand. The proximal joint is a pin joint, and the distal joint is a flexure designed to allow a small amount of out-of-plane twisting in response to inadvertent impacts. The fingers have a single tendon, which travels across both joints before terminating on the rear side of the distal link. The fingertips are flat on the palmar surface, transitioning into a cylindrical tip that is terminated in a thin steel fingernail on the dorsal side. The basic principle of operation of these fingers can be seen by assuming that some tension is applied to the tendon in some configuration. The moment at the proximal joint can be found using the pulley radius of the proximal joint (9 mm), while the approximate moment at the distal joint in the configuration shown will be the tension multiplied by the distance to the neutral axis of the flexure joint (4.25 mm). When this force is applied, the finger will move to equilibrium with the elastic elements (a coil spring at the proximal joint, and the bending stiffness of the distal flexure). Because the distal flexure is significantly stiffer than the proximal spring, and because the moment arm of the tendon over the distal joint is significantly smaller, the fingers preferentially bend at the proximal joint unless the finger encounters an object or obstacle.

The analysis and results presented here will be illustrated using a pair of planar opposed iHY fingers acting in a pinch grasp. This case is easy to envision, and the features that enable stable manipulation are not particularly affected by the transition from two to three dimensions. The principal difference between two and three dimensions is the possibility of non-holonomic rolling contact in three dimensions (Bicchi and Sorrentino, 1995), and the cases where this becomes relevant will be identified as they are encountered.

2.2 Model and terminology

On an abstract level, the mechanics of any grasping problem can be expressed using a generalized coordinate system that represents the free motion of both a hand and a grasped object. Figure 4 illustrates the two-finger pinch grasp considered here, and defines a set of coordinates, q, which is a concatenation of the hand configuration coordinates, θ, and the object configuration coordinates, u:

$$q = \begin{bmatrix} \theta \\ u \end{bmatrix} \tag{1}$$

This hand–object system will be assumed to have a potential function, $V(q)$, describing the elasticity of the hand joints, gravitational forces and any constant disturbance forces on the hand or object. The contact constraints between the hand and a grasped object can be written in terms of a constraint Jacobian, $\Omega(q)$, limiting the relative local motion of the hand and object, δq:

$$\Omega(q)\delta q = 0 \tag{2}$$

Because the actuators used in the iHY hand (and many other hands) use a highly geared transmission, they will be assumed to act on this system as a set of constraints

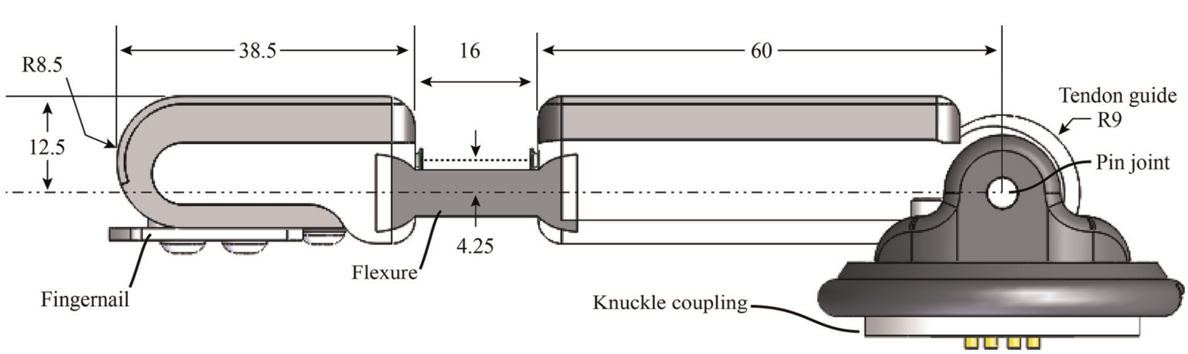

Fig. 3. The fingers of the iRobot–Harvard–Yale Hand. All units are in millimeters.

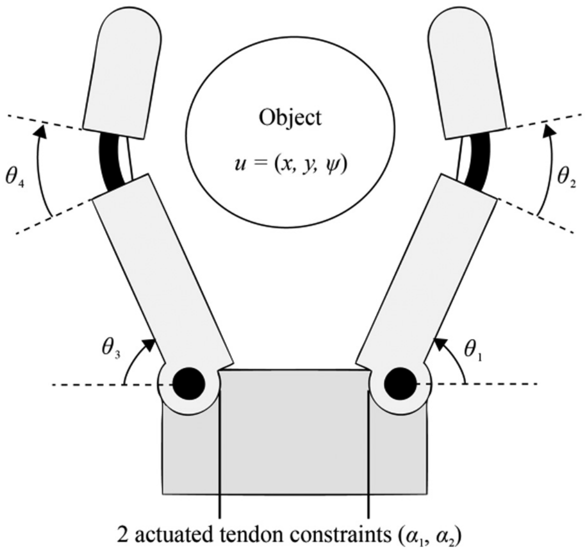

Fig. 4. The planar subset of the iRobot–Harvard–Yale fingers will be modeled as having four degrees of freedom, and an unconstrained planar object has three. The two flexor tendon actuators are treated as constraints.

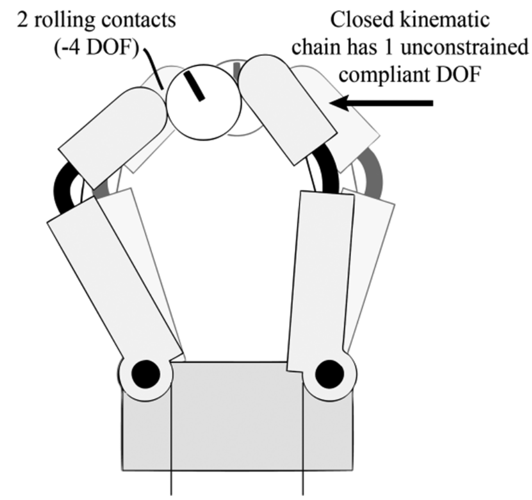

Fig. 5. A pinched object still has one degree of freedom, but this is stabilized by the elasticity of the fingers.

relating the rigid actuator displacement, α, to the hand configuration, q, via the actuator Jacobian, $A(q)$:

$$A(q)\delta q = \delta\alpha \tag{3}$$

The actuation Jacobian will, in practice, depend only on the hand coordinates, but it is convenient to write (3) in this form so that the all of the constraints on the hand can be combined into a single expression relating a perturbation of the hand and object to a change in actuator position:

$$\begin{bmatrix} \Omega(q) \\ A(q) \end{bmatrix} \delta q = \begin{bmatrix} 0 \\ \delta\alpha \end{bmatrix} \tag{4}$$

3. From underactuated grasping to manipulation

So far, the iHY Hand has been introduced and a prototypical experiment has been proposed for underactuated in-hand manipulation and grasping, namely, planar manipulation in a pinch grasp with two opposed iHY fingers. Now we will show how the success criteria for pinch grasping and in-hand fingertip manipulation can be translated from classical sufficient conditions expressed in generalized coordinate form into less rigorous (but more useful) tools for design.

3.1. Pinch grasping with underactuated fingers

As mentioned in Section 1, underactuated grippers tend to obtain power grasps by exploiting the passive hand–object constraints to resist disturbance forces. This can be formally examined by considering the conditions for equilibrium on the hand and object, derived from the definitions in Section 2.1 through the principle of virtual work:

$$\tau = \begin{bmatrix} \tau_{hand} \\ \tau_{obj} \end{bmatrix} = \nabla_q V(q) + \begin{bmatrix} \Omega(q) \\ A(q) \end{bmatrix}^T \begin{bmatrix} \lambda \\ \mu \end{bmatrix} = 0 \tag{5}$$

The balance of generalized forces, τ, includes elastic reaction forces represented in the gradient of the potential energy, $\nabla_q V(q)$, as well as gravity and any modeled constant disturbance force. In order for (5) to be satisfied in a grasp, some set of contact constraint forces, λ, and actuator forces, μ, must be found that exert an equal and opposite generalized force upon the system. This will be possible if the number of independent rows in the combined constraint matrix is equal to or greater than the dimension of the generalized coordinates. Another way of saying this is that the actuators and hand–object contacts must exactly constrain or overconstrain the hand–object system.

Pinch grasping and manipulation with underactuated fingers differs from power grasping in the respect that the contacts between the fingertips and a pinched object may be insufficient to fully constrain the system. Figure 5 depicts the planar iHY Hand grasping a small object. The seven degrees of freedom (7-DOF) hand and object system is constrained by two no-slip rolling contacts removing two DOFs each, and two actuators removing one DOF each, leaving the closed-loop chain formed by the pinch grasp with a mobility of 1. The remaining degree of freedom in the pinching configuration is shown in Figure 5 by the deformation in response to a lateral force on the grasped object. Because the hand and object are no longer fully constrained, the stability criteria for power grasping must be extended to consider compliant motion (Hanafusa and Asada, 1977; Kragten and Herder 2010; Prattichizzo et al., 2012a). As in the power grasping case, the stability criteria relate back to the equations of motion in generalized coordinates. In some configuration, q, a pinched object will be in equilibrium if the sum of the forces is equal to zero as in (5), with sufficient normal force to satisfy any assumption about contact constraint. In addition, any motion resulting from some perturbation $\delta\tau$ must require positive external work. The relationship between a small perturbation force and the resulting change in configuration can be calculated by taking the total derivative of (5) with respect to q, λ and μ:

$$\delta\tau = S(q)\delta q + \Omega(q)^T\delta\lambda + A(q)^T\delta\mu \tag{6}$$

The pseudo-stiffness matrix, $S(q)$, is the gradient of the left-hand side of (5) with respect to q:

$$S(q) = \nabla_q\nabla_q V + \sum_i \nabla_q\Omega_i(q)^T\lambda_i + \sum_i \nabla_q A_j(q)^T\mu_j \tag{7}$$

Here $\Omega_i(q)$ and $A_j(q)$ are the columns of the constraint Jacobian, which are multiplied by their corresponding scalar constraint forces. If we consider some motion δq^* satisfying the constraints, that is, $\Omega(q)\delta q^* = 0$ and $A(q)\delta q^* = 0$, we can obtain an expression for the work resulting from deformation by left-multiplying δq^* into (6):

$$\delta q^{*T}\delta\tau^* = \delta q^{*T}S(q)\delta q^* + \delta q^{*T}\Omega(q)^T\delta\lambda + \delta q^{*T}A(q)^T\delta\mu \tag{8}$$

According to (2) and (3), the terms associated with a change in constraint force will vanish because the motion is in the null space of the contact and actuation Jacobians. Therefore, the work associated with the perturbation can be computed in terms of the pseudo-stiffness matrix, and must be positive:

$$\delta q^{*T}\delta\tau^* = \delta q^{*T}S(q)\delta q^* > 0 \tag{9}$$

Although the conditions in (5) and (9) fully define the necessary conditions for stable pinch grasping, these equations are difficult to use in practice, either for hand design or for the execution of a successful grasp. Too much detailed knowledge of the hand and object are required to accurately model any special case, such as the location of the hand–object contacts, the shape of the object at each contact point and the Jacobians and Hessians of these locations and shapes. Instead of attempting to optimize the hand based on these criteria directly, three rules for design can be considered that will reasonably ensure that pinch grasping is stable:

any unconstrained motion of the hand and object must be associated with an elastic element to provide a restoring force;
the passive elastic restoring forces should provide significant normal force to ensure a stable grasp;
the contact force at each finger in the anticipated use case should not be aligned with the finger's instant center of compliance.

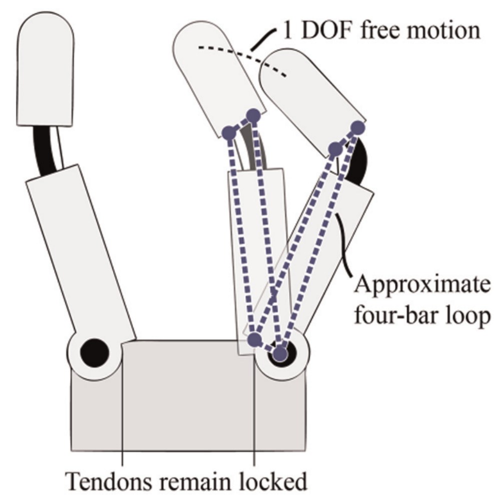

Fig. 6. The behavior of a two-link differentially underactuated finger is approximately equivalent to a four-bar linkage, because the tendon closes the loop between the palm, the proximal link and the distal link of the finger.

These rules relate to the mathematical conditions for stability through the observation that most of the causes of instability just outlined – rank insufficiency due to a non-convex energy Hessian, failure of the physical assumptions underlying frictional constraints and buckling – can be predicted from a few dominant phenomena in the finger mechanics. The first rule is based on the observation that tuning the Hessian of the potential energy, $\nabla_q\nabla_q V$, is the most expedient way of making sure that $S(q)$ is convex in the directions of unconstrained motion. This unconstrained motion can be visualized graphically, by thinking of the iHY finger as a parallel closed chain when the tendon is held fixed. In this configuration, the tendon closes the serial chain comprised of the palm and the proximal and distal phalanges, effectively forming a four-bar linkage, as illustrated in Figure 6. The shearing motion of the parallel four-bar will give the distal link of the finger a one degree of freedom (1-DOF) free trajectory. In order to ensure that this motion has associated elastic energy, the proximal and distal finger joints must be connected in parallel with elastic elements – a torsional spring at the proximal joint and an elastic flexure at the distal joint.

The second design rule relates to the first, insofar as the force produced at the fingertips of an underactuated finger will be partly determined by the finger's passive mechanics. In order to satisfy the frictional conditions of the contact constraints defined in (2), the normal force on a grasped object must be positive and it must be sufficient to maintain frictional contact. This reduces mainly to ensuring that the elastic elements on the proximal and distal joints of each finger are stiff enough that a significant amount of fingertip force is generated. The iHY Hand was designed to exert approximately 10 N on a pinched object (Odhner et al., 2014).

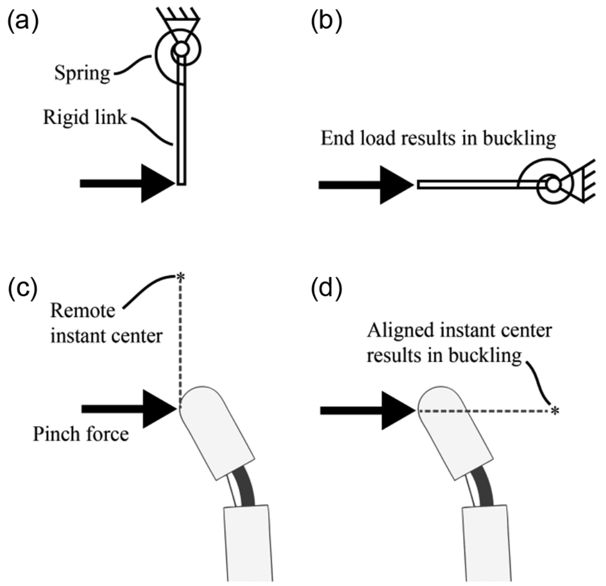

Fig. 7. The instant center of each fingertip's motion will determine whether an underactuated pinch grasp will exhibit incipient buckling behavior.

The third design rule relates to buckling, and thus to the convexity of the pseudo-stiffness $S(q)$ in directions of unconstrained motion as a function of constraint forces. As defined in (7), $S(q)$ is a sum of the Hessian of the potential energy and the Hessian of each constraint multiplied by the corresponding constraint force. If one or more of the constraint forces is large enough to result in a dominant negative eigenvalue in the corresponding constraint Hessian, there is a possibility that the positive restoring force exerted by passive springs could be cancelled out by negative kinematic stiffness in the constraints. The clearest geometric example of buckling is a stiff cantilevered beam, pinned at one end with a parallel torsional spring. This mechanism is not at risk of buckling when subjected to a side load, as shown in Figure 7(a). However, any load directly in line with the pin joint as in Figure 7(b) will, at some critical magnitude, cause the hinged beam to suddenly flop to one side or the other. The stability of the fingertips can be imagined in exactly the same way. Because the iHY finger acts as a four-bar mechanism when the flexor tendon is locked, the distal finger link will have an instant center of motion or compliance that strongly resembles the simple single-link mechanism for the purpose of predicting buckling. Under the anticipated use case (pinch grasping), the internal forces on the fingertips will be primarily normal to the fingertip. An instant center of rotation placed distally to the fingertip will cause more or less linear deformation under load without buckling, just as a side-loaded beam would. An instant center placed behind the fingertip to create an "equilibrium point" on the finger (Birglen et al., 2008; Balasubramanian et al., 2012) will rigidly resist motion of the fingertip, but may buckle unpredictably if a critical pinch force threshold is reached. Even if the modeled higher-order mechanics of pinching in line with the equilibrium point are stable, it is still possible that buckling will occur due to some unmodeled compliant mode, such as twisting (Pounds and Dollar, 2010). The iHY fingers were designed to have a remote center of distal fingertip rotation, which can be seen from the almost-parallel nature of the finger's equivalent four-bar mechanism in Figure 6. This choice ensures that variation in pinch grasp force due to the unknown size or shape of an object minimizes the risk of destabilizing the grasp through buckling.

3.2. From pinch grasping to manipulation

The leap from pinch grasping to manipulation is a short one, and can be analyzed using very standard derivations of the equations of motion. However, using this analysis to determine applicable rules for hand design is challenging and novel. In the previous section, we showed that quasi-static pinch grasp stability could be examined by considering the instantaneous mechanics of the hand and object when the tendons are held fixed; analysis of manipulation, when the tendons are moving, requires that the effect of varying the tendon constraints as in (4) be combined with the second-order stability criteria derived from (6) to form a single linear system:

$$\begin{bmatrix} S(q) & \Omega(q)^T & A(q)^T \\ \Omega(q) & 0 & 0 \\ A(q) & 0 & 0 \end{bmatrix} \begin{bmatrix} \delta q \\ \delta\lambda \\ \delta\mu \end{bmatrix} = \begin{bmatrix} \delta\tau \\ 0 \\ \delta\alpha \end{bmatrix} \tag{10}$$

If the object is to be manipulable, meaning there is a smooth relationship between actuator motion and object motion, this system of equations must be solvable. To show that that the matrix in (10) is invertible, it is sufficient to assert that the stability criterion from (9) must be satisfied, and that the constraint matrix in (4) has full row rank.

Proof. A square matrix is invertible if the result of multiplication by any nonzero vector is also nonzero. Because of the zeroes in the lower-right quadrant of the matrix in (10), two cases need to be considered, the case where $\delta q \neq 0$ in the arbitrary vector multiplied into the matrix, and the case where $\delta q = 0$.

Case 1. If $\delta q \neq 0$, the top block row of (10), $S(q)\delta q + \Omega(q)^T\delta\lambda + A(q)^T\delta\mu$, and bottom two block rows, $\begin{bmatrix} \Omega(q) \\ A(q) \end{bmatrix}\delta q$, cannot simultaneously be zero. That this never happens can be proved by contradiction. We can suppose that the bottom rows are equal to zero, that is, the perturbation of configuration coordinates lies in the nullspace of the constraint matrix. If so, then the same argument used in (8) can be used to show that the top rows will always be nonzero. The value of δq can be transposed and left-multiplied into the top row. The terms containing the constraint forces will vanish, and the remaining term will be positive by our previous assertion in (9).

Case 2. If $\delta q = 0$, the top block row alone will determine the magnitude of the product:

$$\begin{bmatrix} \Omega(q)^T \delta\lambda + A(q)^T \delta\mu \\ 0 \\ 0 \end{bmatrix} \tag{11}$$

This expression will always be nonzero if and only if the transposed constraint matrix $\begin{bmatrix} \Omega(q)^T & A(q)^T \end{bmatrix}$ has rank equal to the number of columns. In other words, all of the constraints on the hand and object must be linearly independent. ■

If both of the above conditions are satisfied, then (10) can be solved for δq, $\delta\lambda$ and $\delta\mu$ omitting the column in the inverted matrix that is multiplied by zero motion in the direction of the contact constraints:

$$\begin{bmatrix} \delta q \\ \delta\lambda \\ \delta\mu \end{bmatrix} = \begin{bmatrix} C(q) & M(q) \\ L_\lambda(q) & K_\lambda(q) \\ L_\mu(q) & K_\mu(q) \end{bmatrix} \begin{bmatrix} \delta\tau \\ \delta\alpha \end{bmatrix} \tag{12}$$

This matrix describes many important properties of the hand for fingertip manipulation. The top row governs the relationship between the configuration of the hand and object, external forces and actuator motion:

$$\delta q = C\delta\tau + M\delta\alpha \tag{13}$$

The matrix $C(q)$ represents the generalized compliance of the hand and object. Actuator motion will affect the configuration of the system through the mobility matrix, $M(q)$. The number of instantaneous motions available to the hand will naturally be limited by the number of actuators; consequently, a two-actuator hand like the iHY Hand will be able to reach a two-dimensional object workspace within the hand. The bottom rows of (12) are equally important, and describe the effect of the actuator motion on the magnitude of the constraint stiffness:

$$\delta\lambda = L_\lambda\delta\tau + K_\lambda\delta\alpha \;\; \delta\mu = L_\mu\delta\tau + K_\mu\delta\alpha \tag{14}$$

Here L_λ and L_μ represent the transmission of perturbation forces to the fingertip contacts and actuators. The contact and actuation stiffness matrices, K_λ and K_μ, are impedance-like terms that govern how much the constraint forces on the hand will change as a function of actuator motion. The contact stiffness matrix K_λ is especially critical to understanding stability in manipulation because it determines the uncertainty in predicting contact force arising from actuated motion. If the stiffness of a contact constraint is large relative to the constraint's magnitude, then it is quite possible for a small perturbation of the actuators to cause the fingertip to lose contact, or to crush the object.

As seen before in the analysis of pinch grasping, the generalized coordinate model provides a convenient framework for proving properties of manipulation with underactuated fingers, but the same problems of knowledge and measurement make design difficult. Calculation of Jacobians and Hessians relies on a priori unknowable quantities, such as detailed object surface geometry. However, the general implications of conditions such as the invertibility of (10) and the contact stiffness matrix K_λ can be visualized and used to improve task performance. The proof above showed that in addition to the criteria for stable pinch grasping, manipulability is predicated on the independence of all hand and object constraints. In practice, this means that the hand and object must be underconstrained or exactly constrained. Figure 5 showed how a simple process of counting the number and kind of contact constraints (i.e. Chebyshev–Grubler–Kutzbach mobility (Rico and Ravani, 2007)) can be used to estimate the hand mobility; because the net mobility of a planar pinch grasp is 1, the object is manipulable, albeit on some two-dimensional manifold due to the limited number of actuators. The added degree of mobility makes the pinch grasp more compliant, but also more robust to changes in contact condition. For example, a no-sliding contact would exert three independent constraints on the normal, shearing and rotation motion between an object and fingertip. One no-sliding (–3 DOFs) and one no-slip rolling (–2 DOFs) contact would still leave the hand and object with a net mobility of zero, allowing manipulation. It is also important to note that the iHY Hand avoids overconstraint in three dimensions as well as two. When three fingers are arranged in a tripod grasp, as depicted in Figure 8, the same process of constraint counting indicates zero net mobility, implying that the object is still manipulable (again, on a manifold of dimension equal to the number of actuators used).

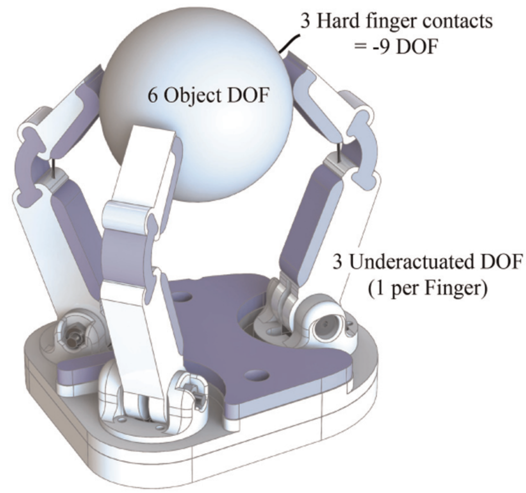

Fig. 8. Preserving the net zero mobility of the full three-fingered hand is vital to enabling fingertip manipulation in three dimensions.

The invertibility of (10) implies that all elements of the contact stiffness matrix K_λ must be finite, but further assurances can be gained by noticing that the principal actuated

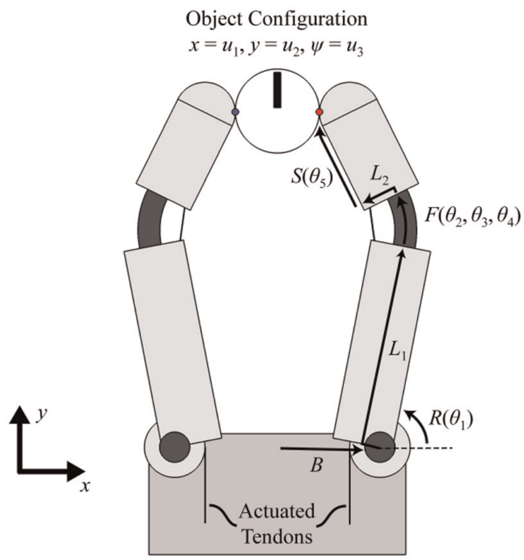

Fig. 9. A schematic model of the hand and a grasped object. Each finger is modeled as having five degrees of freedom (DOFs), including the location of the contact point, and the object is modeled as having three DOFs.

motion of the hand flexes the fingers inward, almost parallel to the direction of four-bar compliance. This is an added benefit of the remote center of fingertip compliance on the iHY Hand. If the fingertips had been designed to be stiff in the direction of the contact normal, contracting a tendon could result in a large increase in fingertip force and consequent buckling, and relaxing a tendon could result in a rapid loss of contact force and consequent loss of contact. Instead, the iHY finger transmission acts as a virtual SEA at the fingertip, so that driving the fingertips into an object causes a smooth increase in force, and so that the fingertips maintain contact with the surface of the object despite uncertainty in object shape or actuation accuracy.

3.3 Example: Two-finger manipulation with the iHY Hand

The criteria for successful fingertip grasping and manipulation have been described algebraically and expressed graphically as rules for hand design. To demonstrate the numerical results of analysis for the iHY Hand, the two-fingered pinching and manipulation criteria were analyzed for the case of a symmetric pinch grasp on a 25 mm diameter round object. In order to ensure that the flexure joints on the fingertips did not introduce buckling modes, a slightly more complex model of the iHY fingers was used for numerical computation instead of the one presented in Section 2.2. The hand and object were modeled as having 13 total degrees of freedom: 3 corresponding to the in-plane position and orientation of the grasped object, and 5 for each finger, as depicted in Figure 9. Instead of the simple model presented in Figure 4, the distal joint of the iHY finger was modeled as a flexure with three principal bending modes using the Smooth Curvature Model (Odhner and Dollar, 2011). The final finger degree of freedom in this model is the distance along the palmar surface of the distal link at which contact is made between the finger and the object. The elastic energy of the hand was computed from the rotational stiffness of the proximal joint, which was measured to be 44 mNm/rad, and the stiffness of the distal joint, which was found to be 195 mNm/rad. The contact position of each finger was calculated by composing the chain of geometric transformations along the length of the finger:

$$X = B * R(\theta_1) * L_1 * F(\theta_2, \theta_3, \theta_4) * L_2 * S(\theta_5) \qquad (15)$$

Here B, L_1 and L_2 are constant homogeneous transformations representing the link-to-link translation between joints. The proximal joint rotation, $R(\theta_1)$, and the distal flexure deformation, $F(\theta_2, \theta_3, \theta_4)$, are functions of the hand coordinates, and $S(\theta_5)$ represents a translation along the surface of the distal link, parameterized in terms of the surface distance of the contact point from the base of the finger, θ_5. The constraints for the two actuated tendons were calculated by finding the configuration-dependent tendon length as a function of the joint variables, based on the free length of tendon over the flexure at the distal joint, and the free length of tendon over the tendon guide on the proximal pin joint, as illustrated in Figure 3. In order to find an initial contact configuration between the fingers and the object, the hand was initially modeled in the absence of contact constraints, and the tendons were pulled until the spacing between the fingertips was equal to the diameter of the grasped object. The fingertips were then constrained to the surface of the object using rolling constraints, by imposing the same distance between initial contact and present position on the contact points, both on the object and on the fingertips. Each contact constraint removed three DOFs from the hand and object, effectively eliminating the contact position variable θ_5 and providing two additional constraints on the fingertips and object.

3.4. Results

The hand model was simulated in Matlab using the Freeform Manipulator Analysis Toolbox (FMAT), a freely available, extendable package that can be obtained from the authors' website. The equilibrium configuration was found for a symmetric pinch grasp, executed by retracting the tendons 2 mm past the point at which initial contact was made with the object. This configuration is shown in Figure 9. The equilibrium configuration was found using a constrained energy minimization, which had the side effect of also checking the convexity of the energy around the solution, verifying the stability of the grasp without additional computation. The system in (10) was computed, and from this compliance and mobility of the grasped object were found using (12). The rows and columns of $C(q)$

corresponding to motion of the grasped object in response to force on the object were computed:

```
queue = {(α_0, q_o)}
visited = {}
stable_cfgs = {}
while size(queue) > 0:
for (α_i, q_i) in queue :
q*, λ*, μ* = solve_(20)_with_guess(q_i)
   if g(q*, λ*, μ*):
      append (α_i, q*, f(λ*)) to stable_cfgs
      for α_j in adjacent_grid_points(α_i):
         if α_i ∉ visited and α_i ∉ queue :
            append (α_j, q*) to queue
   remove (α_i, q_i) from queue
   append α_i to visited
```

$$\begin{bmatrix} \delta x \\ \delta y \\ \delta \psi \end{bmatrix} = \begin{bmatrix} 9.98 & 0.00 & -.0918 \\ 0.00 & 0.0109 & 0.00 \\ -.0918 & 0.00 & 0.00127 \end{bmatrix} \begin{bmatrix} \delta f_x \\ \delta f_y \\ \delta \tau_\psi \end{bmatrix} \qquad (16)$$

Here displacements are measured in mm, forces in N, angles in rad and moments in mNm in the coordinate frame shown in Figure 10. Because the chosen pinch grasp is symmetric, it is unsurprising that there is no cross-coupling between y motion (perpendicular to the palm) and translation or rotation. The coupling between x (lateral) motion and rotation is also expected; the object will roll back and forth on the fingertips, so a lateral force will cause some rotation, and vice versa. The rows of $M(q)$ corresponding to the motion of the object under a change in tendon length were computed from (12):

$$\begin{bmatrix} \delta x \\ \delta y \\ \delta \psi \end{bmatrix} = \begin{bmatrix} 4.11 & -4.11 \\ 1.85 & 1.85 \\ 0.962 & -0.963 \end{bmatrix} \begin{bmatrix} \delta \alpha_1 \\ \delta \alpha_2 \end{bmatrix} \qquad (17)$$

The tendon lengths are also measured in mm. Again, the symmetry of the grasp configuration can be observed in the result. Increasing either tendon length, thereby opening the hand, results in motion in the palmar direction $(+y)$, while the lateral motion produced by moving the tendons is coupled to the rotation of the object. The instantaneous change in constraint forces resulting from actuator motion was found from (12):

$$\begin{bmatrix} \delta \lambda_{S1} \\ \delta \lambda_{N1} \\ \delta \lambda_{S2} \\ \delta \lambda_{N2} \end{bmatrix} = - \begin{bmatrix} 0.020 & 0.018 \\ 0.30 & 0.30 \\ 0.019 & 0.021 \\ 0.30 & 0.30 \end{bmatrix} \begin{bmatrix} \delta \alpha_1 \\ \delta \alpha_2 \end{bmatrix} \qquad (18)$$

The shear forces at the contact points are denoted by λ_S, and the normal forces by λ_N. All units are again in mm and N. Asymmetry in the force sensitivity is not explained by the symmetric configuration of the tendon actuators, and must be attributed to numerical error in the minimization method used to compute the equilibrium configuration. One notable feature of the constraint force sensitivity matrix is that the rates at which the normal forces increase as the tendons are pulled are much larger than the rates at which shear forces increase. This is desirable if the grasp is to remain stable as the tendons are further contracted.

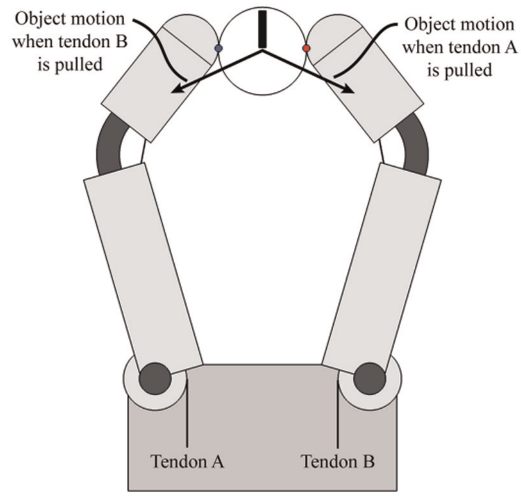

Fig. 10. The finger in a symmetric pinched configuration. Arrows denote the direction of xy object motion as the tendons are shortened.

3.5. Summary

The classical algebraic conditions for equilibrium and stability in the generalized manipulator equation carry specific meaning for the problem of designing underactuated hands. In this section, we showed that tuning the four-bar linkage behavior of the actuated finger is crucial for satisfying the formal success criteria of pinch grasping and fingertip manipulation. By carefully choosing the fingertip compliance and the instant center of underactuated finger motion, instabilities such as buckling can be avoided, and compliant contact with a manipulated object can be ensured while the actuators are moving. The importance of avoiding overconstraint in manipulation was proved, and the practicality of the iHY Hand for two- and three-dimensional fingertip manipulation was demonstrated.

4. Predicting global manipulability

Now that a method for determining the local stability and manipulability of an underactuated grasp has been introduced, we turn to the problem of determining the global range of motion that a grasped object can undergo starting from some initial grasp. If each finger of the hand is fully actuated, then it is possible to analyze the manipulable workspace by examining each finger separately. However, in an underactuated hand, this is not the case. The kinematics of the hand and grasped object must be considered holistically, as one might analyze a parallel platform, to determine the range of object motion.

In this section, we demonstrate an algorithm for mapping out all possible object positions that can be reached from some initial grasp configuration, assuming that the pinched object has relatively simple surface geometry. In the previous section we remarked that the equilibrium configurations of the hand and object are aptly described as a manifold, that is, a subset of all possible configurations on which local motion is restricted to a lower-dimensional space corresponding to the motion of the actuators. This manifold structure is important for determining the configurations that can be reached, because "reaching" some target configuration from an initial grasp involves finding a trajectory of actuator inputs that can keep the object in a stable grasp while it is moved. We will approach the problem by discretizing the space of local motions to fixed-magnitude changes in actuator input. The discretized space can be explored as a graph, starting from the node corresponding to the initial grasp. When exploring each neighboring node of this graph, the equilibrium configuration of the hand will be found by finding the local energy minimum produced by varying the actuator constraints. The criteria from Section 3 for stability can be used to test the stability of this new configuration. The end result, an approximation to the manifold of reachable configurations, can be visualized and used as a design tool to understand a priori the manipulation capabilities of an underactuated hand.

4.1. Solving for local minimum-energy configurations

Given some set of actuator inputs for a hand, the corresponding configuration of a hand and object can be solved by minimizing the hand and object potential energy $V(q)$, bound by contact and actuation constraints that can be expressed globally:

$$\omega(q) = 0 \qquad a(q) = \alpha \tag{19}$$

The instantaneous constraints from (2) and (3) can be written in this form if they are integrable, which is only sometimes the case for three-dimensional contact constraints. Many contact constraints can be approximated as holonomic constraints (for example, as pin joints, ball-and-socket joints or two-dimensional rolling contacts). For cases in which the non-holonomy cannot be neglected, other frameworks for predicting global manipulability, such as geometric controllability, may be more appropriate (Murray et al., 1994; Bicchi and Sorrentino, 1995; Srinivasa et al., 2002). When the constraints are holonomic, it is possible to find the equilibrium configuration of the hand for any actuator configuration by minimizing the internal energy in the hand–object configuration:

$$q^* = \arg\min_{q,\lambda,\mu} V(q) + \omega(q)^T\lambda + (a(q) - \alpha)^T\mu \tag{20}$$

Equation (20) could be seen in some ways as a nonlinear pseudo-inverse to (19), a function mapping some actuator input α onto a configuration of the hand and object while minimizing the energy in directions not specified by the constraints.

4.2. Testing stability

The minimum-energy solution q^* and its associated constraint forces, λ^* and μ^*, describe a valid grasp only if the stability conditions discussed in Section 3.1 are met, including conditions determining the validity of the constraints. Some of these conditions are Boolean conditions, such as the requirement that a normal constraint cannot support a tension force. Limits of actuator and joint travel will provide an additional set of Boolean conditions governing the validity of a minimum-energy solution. All of these will be lumped into a single Boolean function $g(q^*, \lambda^*, \mu^*)$ that is true if all criteria are met.

Coulomb friction stability conditions are difficult to ascertain in a binary fashion because the contact properties of different materials vary widely. To account for this, a scalar cost function $f(\lambda^*)$ must also be defined, determining the maximum coefficient of friction needed to keep any particular manipulation configuration stable:

$$f(\lambda^*) = \max_i \left(\frac{|\lambda^*_{S,i}|}{|\lambda^*_{N,i}|} \right) \tag{21}$$

Here $\lambda^*_{S,i}$ and $\lambda^*_{N,i}$ are the shear and components of the ith contact constraint force. Using these two functions, one can test any equilibrium configuration to determine whether it should be included in the set of configurations to which an object can be manipulated.

4.3. Grid mapping

Equipped with a set of automated criteria for validating the stability of a grasp, we turn to the problem of exploring the whole manifold of reachable object configurations using a discretized search algorithm. Initially, some grasping configuration is known, and this known stable configuration q_o combined with the corresponding actuator input α_0 will be assigned as the root node in the graph of reachable configurations. From here, the graph is extended by incrementing or decrementing each of the actuators by a set amount, as illustrated in Figure 11. The equilibrium configuration for each new node is found, and if the solution corresponds to a stable grasp, it is added to the graph of reachable configurations. The following pseudo-code describes the process in detail:

Each actuator input α_i is tested to see if it corresponds to a valid grasp. If it does, then it is appended to the set of

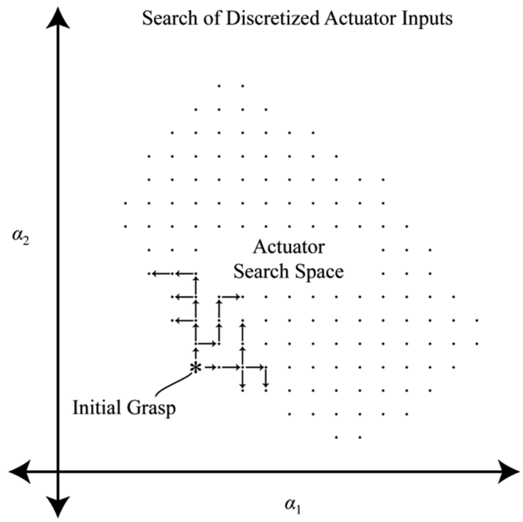

Fig. 11. The manifold of reachable hand/object configurations starting with an initial grasp can be approximated by exploring a grid of actuator inputs.

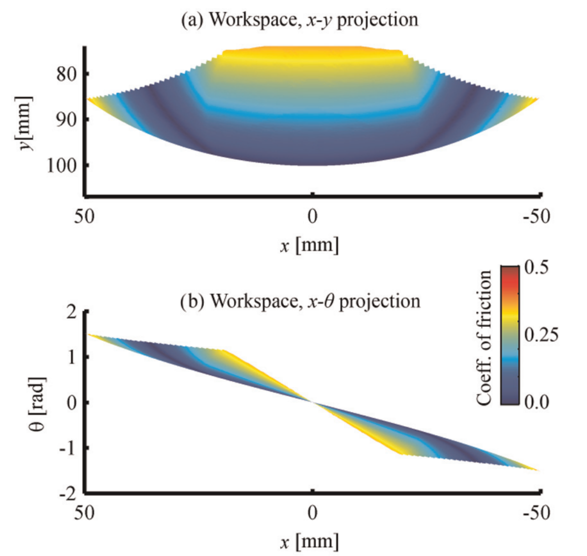

Fig. 12. Visualization of the reachable workspace of a 20 mm diameter cylindrical object grasped between two iRobot–Harvard–Yale fingers. The shading shows the minimum friction coefficient required for stability.

stable configurations, and a set of adjacent actuator inputs is generated to expand the search region in the actuator space. This is done by adding a fixed increment to one row of α_i. Minimizing the energy of the hand and object at every point using an initial guess from an adjacent configuration has two advantages: firstly, it speeds up convergence of the energy minimization significantly. It also has the advantage of ensuring local connectivity by starting near a local minimum, so that if more than one stable configuration can be found, the correct solution is used, that is, the solution that can be reached from the specific initial grasping configuration chosen. The use of local initial conditions does raise the possibility of path dependence in the solutions found; however, this tends not to happen if the hand mechanism is not near buckling, where such bistable behavior can be found. Section 3.1 presents other reasons why these situations should be avoided. If it is desirable to limit the manifold found in this way to a specific range of frictional coefficients, then the algorithm can be augmented to discard points for which $f(\lambda^*)$ is greater than the maximum coefficient of friction.

4.4. Example: Two-finger manipulation with the iHY Hand

As an example, the reachable configuration manifold of the planar iHY Hand was computed. The fingers were preconfigured for an initial grasp by moving them inward until the fingertip spacing was exactly one diameter of the grasped object. To find the initial stable configuration from which the manifold was explored, the tendons were contracted slightly from the starting point, so that some small positive normal force was exerted on the fingertips. The finger lengths were then varied using the algorithm just described. The resulting set of stable object configurations was converted into a meshed surface, and projected into the object coordinates shown in Figure 12. The first important result is that the object range of motion is fairly large, spanning approximately 100 mm in the x direction (parallel to the palm) and 30 mm in the y direction (perpendicular to the palm). The lateral and angular motion is strongly coupled, so that the object can be rotated approximately 1 radian by rolling the object from side to side in the grasp. The reachable configuration manifold is shaded using the scalar stability criterion, $f(\lambda^*)$. This indicates that the coefficient of friction needed to maintain contact is reasonable in magnitude throughout the region shown. If the coefficient of friction between the fingers and the object were small, then the size of the reachable configuration manifold would shrink, moving along the level curves of $f(\lambda^*)$ corresponding to the coefficient of friction.

All possible trajectories of a manipulated object will lie on the interior of the computed manifold. For example, Figure 13 shows a simulated task in which the round object is grasped and twisted. The actuators are first co-contracted to bring the object into a tight pinch, and then the object is rolled to the side by further contracting one tendon while lengthening the other. The object is released by lengthening both tendons at an equal rate. Four hand poses along this trajectory are shown to visualize the relationship between the path in actuator coordinates and the path in object coordinates. The manipulation trajectory highlights an interesting side effect of the relationship between hand configuration and fingertip force. When the object is released by the fingertips, it inevitably has to travel to the edge of the manifold corresponding to the configurations in which a stable grasp is no longer achieved, such as when the fingertip normal force goes to zero. For the example given, these configurations occur only on edge of the

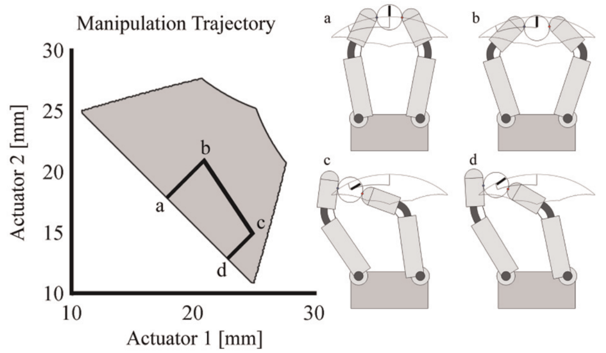

Fig. 13. An example manipulation task, in which the object is pinched, rolled to one side, and then released. The x–y projection of the reachable configuration manifold is shown superimposed on four snapshots along the finger trajectory, labeled a–d.

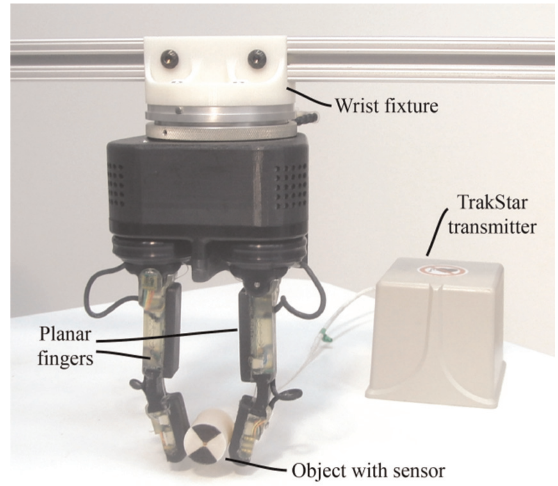

Fig. 14. To measure the workspace of a 20 mm diameter object, the iRobot–Harvard–Yale Hand was mounted to a fixture above a table. A TrakStar electromagnetic position tracking system was used to record the object's position.

workspace furthest from the hand. Hands with a larger number of actuators may be able to release a grasped object over a wider range of configurations. A good example would be the case of hands with SEAs at every joint, which can control force while holding the position constant (Prattichizzo et al., 2012a). Such hands are still underactuated in the sense that the SEAs add many internal degrees of freedom to the hand, associated with the stretch of each elastic element. However, because the manifold of reachable configurations has a higher dimension (often higher than the number of object degrees of freedom), the projection of the reachable configuration manifold onto the space of object configurations will show that many different fingertip forces can be achieved at each configuration.

4.5. Experimental workspace measurement

To demonstrate the kind of predictive accuracy that can be expected from a model-based prediction of workspace, measurements of manipulation trajectories were combined to form a map of the workspace for the 20 mm diameter cylinder whose workspace was computed. An iHY Hand was mounted to a static fixture above a flat table surface, as depicted in Figure 14. This hand was held close enough to the table that the tips of the fingers could grasp the cylindrical object from the tabletop. A TrakStar magnetic position tracking system (Ascension Technologies) was placed on the table top next to the hand, and a single tracking marker was glued into the center of the cylinder. To measure the workspace of the object, a sequence of actuation and measurement steps was performed:

- the fingers were opened slightly, so that the object was resting on the table;
- the fingers were closed into a light pinch grasp position (shown in Figure 14);
- the TrakStar sensor measured the position and orientation of the object;
- the finger tendons were moved to pre-set tendon lengths on a straight-line path (in tendon space);
- the TrakStar sensor was used to measure the relative position and orientation of the object from the initial pinch grasp;
- the object was returned to a pinch grasp to reset the experiment.

This sequence of steps produced a grid of planar homogeneous transformation matrices defining the relative motion imposed on the object as a function of actuator commands. The object was dropped and regrasped after every measurement to avoid slow error accumulation due to slippage. If the object was ejected from the grasp, that data point was discarded. The resulting data set is plotted in Figure 15. The object's x–y position was registered with the modeled workspace, and the prediction error between the modeled orientation and the measured orientation was used to shade the results. The fit between model and measurement is very good for lightly pinched objects, but degrades as the object is drawn inward into the hand. The errors are most likely a result of inaccuracy in predicting the distal joint travel limits, due to rubbing that was observed between the elastomer pads on the proximal and distal joints. The other possible source of error was slippage due to increasing internal forces.

4.6. Summary

The chief advantage of using an underactuated hand for in-hand manipulation is the passive stability that results from properly tuned finger mechanics. In exchange for a more limited space of reachable object configurations, the iHY Hand is capable of repositioning an object within the hand

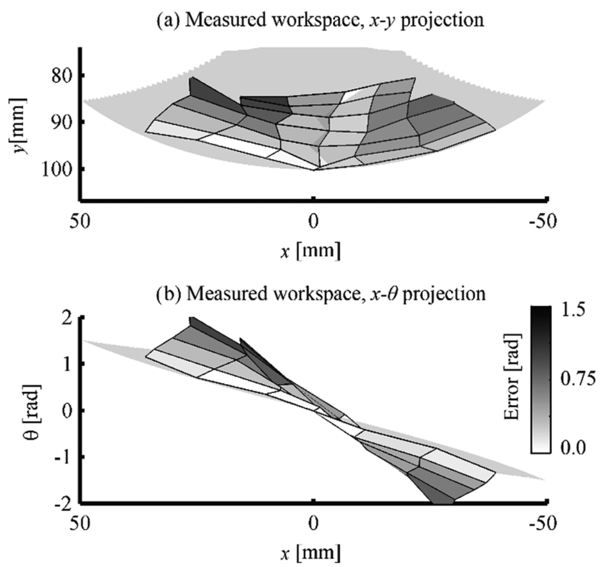

Fig. 15. The measured workspace of the object is shown superimposed on the computed workspace. Significant errors in predicting the object's rotation occur near the inward joint travel limits of the distal joint.

over an area approximately 20 mm by 80 mm. No feedback control is needed to achieve this capability.

We have shown that the manifold of reachable object configurations can be numerically approximated via grid search for hands having holonomic contact constraints. Because it is possible to compute this a priori, the capabilities of an underactuated hand can be tested during the design process, much in the same way that one might analyze the workspace of a serial manipulator. The experimental results showed that the model produces approximately the expected result, but will be sensitive to assumptions about the kinematics of the fingers and object. Because the shape of real objects will rarely be known with a sufficient degree of accuracy for modeling, we do not see this tool as a method for control; however, techniques in visual servoing and machine learning can undoubtedly be layered on top of the passively stable behavior to achieve better positional accuracy.

5. Conclusions

Although in-hand manipulation is a difficult problem, the mechanics of holding an object in an underactuated gripper dictate a set of conditions under which in-hand manipulation is not only feasible, but also relatively easy in the absence of high-fidelity sensory feedback. We have shown how a few basic rules related to the compliant behavior of differentially underactuated fingers can be followed in order to achieve stable grasping and local manipulability, and have experimentally demonstrated a robot hand having an in-hand workspace large enough to be of use in performing real-world tasks.

Acknowledgements

Preliminary portions of this work were presented at the 2011 IEEE International Conference on Robotics and Automation (Odhner and Dollar, 2011) and the 2012 International Symposium on Experimental Robotics (Odhner et al., 2013).

Funding

This work was supported in part by the National Science Foundation (grant IIS-0953856) and by DARPA (grant W91CRB-10-C-0141).

References

Aukes DM, Heyneman B, Ulmen J, et al. (2014) Design and testing of a selectively compliant underactuated hand. *The International Journal of Robotics Research* 33(5): 721–735.

Balasubramanian R, Belter JT and Dollar AM (2012) Disturbance response of two-link underactuated serial-link chains. *Journal of Mechanisms and Robotics* 4(2): 021013.

Bicchi A and Sorrentino R (1995) Dexterous manipulation through rolling. In: *Proceedings of the 1995 IEEE international conference on robotics and automation*, May, IEEE, Vol. 1, pp. 452-457.

Birglen L, Gosselin C and Laliberté T (2008) *Underactuated Robotic Hands*. Vol. 40. Berlin: Springer, p.13.

Crisman JD, Kanojia C and Zeid I (1996) Graspar: A flexible, easily controllable robotic hand. *IEEE Robotics & Automation Magazine* 3(2): 32–38.

Dollar AM and Howe RD (2009) The SDM Hand: A highly adaptive compliant grasper for unstructured environments. In: Khatib O, Kumar V and Pappas GJ (eds) *Experimental Robotics*. Berlin, Heidelberg: Springer, pp. 3-11.

Edsinger-Gonzales A and Weber J (2004) Domo: A force sensing humanoid robot for manipulation research. In: *2004 4th IEEE/RAS international conference on humanoid robots*, November, IEEE, Vol. 1, pp.273–291.

Grebenstein M, Chalon M, Friedl W, et al. (2012) The hand of the DLR hand arm system: Designed for interaction. *The International Journal of Robotics Research* 31(13): 1531-1555.

Hanafusa H and Asada H (1977) Stable prehension by a robot hand with elastic fingers. In: *Proceedings of the 7th international symposium on industrial robots*, October, pp. 361–368.

Hirose S and Umetani Y (1978) The development of soft gripper for the versatile robot hand. *Mechanism and Machine Theory* 13(3): 351–359.

Kinova Robotics (2013) JACO. Available at: http://www.kinovarobotics.com/products/jaco-research-edition/ (accessed 26 November 2013).

Kragten GA and Herder JL (2010) The ability of underactuated hands to grasp and hold objects. *Mechanism and Machine Theory* 45(3): 408-425.

Ma RR and Dollar AM (2011) On dexterity and dexterous manipulation. In: *Proceedings of the 2011 IEEE international conference on advanced robotics (ICAR)*, Tallinn, Estonia.

Mason MT and Salisbury JK Jr (1985) *Robot Hands and the Mechanics of Manipulation*. Cambridge, MA: MIT Press.

Michelman P (1998) Precision object manipulation with a multifingered robot hand. *IEEE Transactions on Robotics and Automation* 14(1): 105-113.

Murray RM, Li Z and Sastry SS (1994) *A Mathematical Introduction to Robotic Manipulation*. Boca Raton: CRC Press.

Odhner LU and Dollar AM (2011) Dexterous manipulation with underactuated elastic hands. In: *2011 IEEE international conference on robotics and automation (ICRA)*, May, IEEE, pp. 5254-5260.

Odhner LU, Jentoft LP, Claffee MR, et al. (2014) A compliant, underactuated hand for robust manipulation. *The International Journal of Robotics Research* 33(5): 736-752.

Odhner LU, Ma RR and Dollar AM (2013). Experiments in underactuated in-hand manipulation. In: *Experimental Robotics*. Springer International Publishing, pp. 27-40.

Okamura A, Smaby N and Cutkosky MR (2000) An overview of dexterous manipulation. In: *Proceedings of the 2000 IEEE international conference on robotics and automation, symposium on dexterous manipulation*, Vol. 1, pp. 255–262.

Pounds PE and Dollar AM (2010) Towards grasping with a helicopter platform: Landing accuracy and other challenges. In: *Australasian conference on robotics and automation*, Australian Robotics and Automation Association (ARAA).

Prattichizzo D, Malvezzi M, Aggravi M, et al. (2012a) Object motion-decoupled internal force control for a compliant multifingered hand. In: *2012 IEEE international conference on robotics and automation (ICRA)*, May, *IEEE*, pp. 1508-1513.

Prattichizzo D, Malvezzi M, Gabiccini M, et al. (2012b) On the manipulability ellipsoids of underactuated robotic hands with compliance. *Robotics and Autonomous Systems* 60(3): 337–346.

Quennouelle C and Gosselin C (2009) A quasi-static model for planar compliant parallel mechanisms. *Journal of Mechanisms and Robotics* 1(2): 021012.

Rico JM and Ravani B (2007). On calculating the degrees of freedom or mobility of overconstrained linkages: single-loop exceptional linkages. *Journal of Mechanical Design* 129(3): 301–311.

Robotiq (2013) 3-finger adaptive robot gripper. Available at: http://www.robotiq.com/en/products/industrial-robot-hand/ (accessed 26 November 2013)

Srinivasa S, Baker CR, Sacks E, et al. (2002) Experiments with nonholonomic manipulation. In: *Proceedings of the IEEE international conference on robotics and automation (ICRA), volume 2*, pp. 2042–2047, IEEE.

Ulrich N, Paul R and Bajcsy R (1988). A medium-complexity compliant end effector. In: *proceedings of the 1988 IEEE international conference on robotics and automation*, April, IEEE, pp. 434-436.